On a nonlocal system for vegetation in arid ecosystems

Matthieu Alfaro*, Hirofumi Izuhara† and Masayasu Mimura‡§

July 14, 2017

Contents

Abstract

Several mathematical models are proposed to understand spatial patchy vegetation patterns arising in arid environments. In this paper, we consider the system with nonlocal dispersal (spreading) of plants proposed by Pueyo et al. in [14] as a model for vegetation in arid ecosystems. It consists in two reaction diffusion equations for surface water and soil water, combined with an integro-differential equation for plants. For this system, under suitable assumptions, we prove well-posedness using the Schauder fixed point theorem. In addition, we consider the stationary problem from the viewpoint of vegetated pattern formation, which is associated with catastrophic shifts for desertification.

1 Introduction

In arid environments, vegetation patterns with patchiness such as stripes, spots, labyrinths and gaps are observed [2], [8], [15], [17]. The distance between stripes/spots of the vegetation patterns is wide-ranging from tens of centimeters to hundreds of meters, depending

*IMAG, Université de Montpellier, CC051, Place Eugène Bataillon, 34095 Montpellier Cedex 5, France.
†Faculty of Engineering, University of Miyazaki, 1-1 Gakuen Kibanadai Nishi, Miyazaki, 889-2192, Japan.
‡Faculty of Engineering, Musashino University, 3-3-3 Ariake, Koto-ku, Tokyo 135-8181, Japan
§Meiji Institute for Advanced Study of Mathematical Sciences, Meiji University, 4-21-1 Nakano, Nakano-ku, Tokyo 164-8525, Japan.

on plant species. Moreover, it is also reported that vegetation patterns observed in fields are independent of soil type and specific plant species. Figure 1 shows typical vegetation patterns in arid ecosystems. It is said that the patchiness of vegetation in arid ecosystems

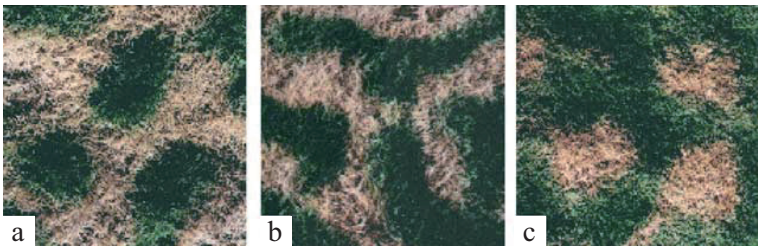

Figure 1: Vegetation patterns of the perennial grass *Paspalum varinatum* in Israel (200mm mean annual rainfall). (a) spots. (b) stripes. (c) gap. The distance between spots/stripes is of the order of 15 cm. Reproduced with permission from [4].

is formed in a self-organized way in water-limited environments and an important signal to catastrophic shifts for desertification [17], [19]. In order to understand such self-organized vegetation pattern formation, a theoretical approach is required, see [2] for instance. For a few decades, a lot of mathematical models to describe the vegetation pattern formation in arid ecosystems have been developed. Klausmeier [9] focused on two important factors, plant density and water concentration, to describe stripe vegetation patterns formed on slopes and proposed a two component reaction-diffusion-advection system. We refer to [20], [21] and the references therein for studies using Klausmeier model. Based on the Klausmeier model, a lot of improvements have been performed. The authors in [5], [13] focus on three factors, plant density, surface water and soil water. The proposed models are reaction-diffusion systems, which include only local effects. They suggest that the vegetation patterns in desertification are generated as a result of the diffusion-induced instability (the Turing instability) [5], [7], [11], [13], [16], [18].

On the other hand, it is not reasonable to describe the spreading of plants as a diffusion term since the latter is based on the random movement of each individual. Each plant establishes, instead, seed dispersal which contributes to the spreading [1]. In this context, Pueyo et al. [14] proposed a new mathematical model with three components, plant density and amounts of soil water and surface water. A feature of this model is to contain a nonlocal term for the plant spreading. It reads

$$\begin{aligned}
\frac{\partial P}{\partial t} &= c_P g_{P_{max}} \frac{W}{W+k_1} P - (d_P + f)P + r_c \frac{W}{W+k_1} g_S \int_\Omega f P(t,y)\Phi(x,y)dy, \\
\frac{\partial W}{\partial t} &= \alpha U \frac{P + k_2 w_U}{P + k_2} - g_{P_{max}} \frac{W}{W+k_1} P - r_W W + d_W \Delta W, \\
\frac{\partial U}{\partial t} &= r_{rain} - \alpha U \frac{P + k_2 w_U}{P + k_2} + d_U \Delta U,
\end{aligned} \tag{1}$$

where $P(t,x)$, $W(t,x)$ and $U(t,x)$ $(t > 0,\ x \in \Omega)$ respectively represent plant density, soil water and surface water at time t and position x. Here, Ω is a connected bounded open set of $\mathbb{R}^N$, with smooth boundary $\partial\Omega$. All the parameter values are positive constants. The equation for the plant density P consists of plant growth and loss, and seed dispersal.

The plant growth depends on amount of soil water $W(t,x)$, described as Michaelis-Mentan kinetics and the plant loss is at a constant rate. The third term of the right hand side in the equation for P describes seed dispersal, germination and establishment. The integral term $\int_\Omega fP(t,y)\Phi(x,y)dy$ means seed density, that is seed is produced by the plant at a constant rate f and is dispersed. Here, the kernel Φ is a probability density function, therefore, we assume that $\int_\Omega \Phi(x,y)dy = 1$ for any $x \in \Omega$. In addition, the term $r_c\frac{W}{W+k_1}g_S$ in front of the integral term means an establishment rate for seedlings, which also depends on soil water. The second and third equations describe the dynamics of water, where water is divided into two stages: soil water and surface water. The constant r_{rain} is rainfall and the term $-\alpha U\frac{P+k_2w_U}{P+k_2}$ represents an infiltration rate from ground into subsurface, which depends on the plant density: plenty of biomass facilitates the infiltration of water ($w_U < 1$). The terms $-g_{P_{max}}\frac{W}{W+k_1}P$ and $-r_W W$ in the equation for W mean the losses of soil water due to uptake by plants and due to drainage and evaporation, respectively. Finally, the dispersal of soil water and surface water is described by diffusion.

In order to reduce the number of parameters, we use the following change of variables (nondimensionalization):

$$
\begin{aligned}
&\tilde{P}(\tilde{t},\tilde{x}) = \frac{1}{k_2}P(t,x), \quad \tilde{W}(\tilde{t},\tilde{x}) = \frac{1}{k_1}W(t,x), \quad \tilde{U}(\tilde{t},\tilde{x}) = \frac{\alpha}{g_{P_{max}}k_2}U(t,x),\\
&\tilde{\Phi}(\tilde{x},\tilde{y}) = \left(\frac{d_U k_1}{g_{P_{max}}k_2}\right)^{N/2}\Phi(x,y),\\
&\tilde{t} = \frac{g_{P_{max}}k_2}{k_1}t, \quad \tilde{x} = \sqrt{\frac{g_{P_{max}}k_2}{d_U k_1}}x, \quad \tilde{y} = \sqrt{\frac{g_{P_{max}}k_2}{d_U k_1}}y,\\
&\tilde{\Omega} = \left\{\sqrt{\frac{g_{P_{max}}k_2}{d_U k_1}}z,\ z \in \Omega\right\},\\
&a = \frac{c_P k_1}{k_2}, \quad b = \frac{(d_P+f)k_1}{g_{P_{max}}k_2}, \quad c = \frac{r_c g_S f k_1}{g_{P_{max}}k_2}, \quad d = \frac{d_W}{d_U}, \quad e_0 = \frac{r_W k_1}{g_{P_{max}}k_2},\\
&r = \frac{\alpha r_{rain}k_1}{(g_{P_{max}}k_2)^2}, \quad g = \frac{\alpha k_1}{g_{P_{max}}k_2}.
\end{aligned}
$$

Then, (1) is recast into

$$
\begin{aligned}
\frac{\partial P}{\partial t} &= a\frac{W}{W+1}P - bP + c\frac{W}{W+1}\int_\Omega P(t,y)\Phi(x,y)dy,\\
\frac{\partial W}{\partial t} &= d\Delta W + U\frac{P+w_U}{P+1} - \frac{W}{W+1}P - e_0 W, \qquad t>0,\ x\in\Omega, \qquad (2)\\
\frac{\partial U}{\partial t} &= \Delta U + r - gU\frac{P+w_U}{P+1},
\end{aligned}
$$

where we have dropped the tildes.

In this paper, since we impose the Neumann boundary conditions for surface water and soil water, the corresponding dispersal kernel is needed. Precisely, we assume the following.

Assumption 1.1 (Dispersal kernel) *Kernel* $\Phi : \overline{\Omega}\times\overline{\Omega} \to [0,\Phi_{max}]$ *is continuous, and satisfies*

$$\Phi(x,y) \geq \Phi_0 > 0 \quad \text{when } |x-y| \leq \delta_\Phi, \qquad (3)$$

for some constants $\Phi_0 > 0$, $\delta_\Phi > 0$, *and, for all* $x \in \overline{\Omega}$,

$$\int_\Omega \Phi(x,y)\,dy = 1, \tag{4}$$

together with

$$D_y\Phi(x,y)\cdot n_y = 0 \quad \text{for all } y \in \partial\Omega,$$

where n_y *is an outward unit normal vector to* $\partial\Omega$ *at point* y.

For instance, in one space dimension $(0, L)$, one can simply think of

$$k(x,y) := \frac{1}{\alpha} e^{-\beta(x-y)^2}, \tag{5}$$

and

$$\Phi(x,y) = \sum_{i=-\infty}^{\infty} (k(x, y+2iL) + k(x, 2iL-y)),$$

where the constant α is adjusted so that $\int_0^L \Phi(x,y)dy = 1$ (see [6]). To perform numerics in Section 4, we shall use the approximation

$$\Phi_{approx}(x,y) = k(x,y) + k(x,-y) + k(x,2L-y).$$

Figure 2 shows a graph of the kernel $\Phi_{approx}(x,y)$. The derivative conditions on the boundary are approximately satisfied.

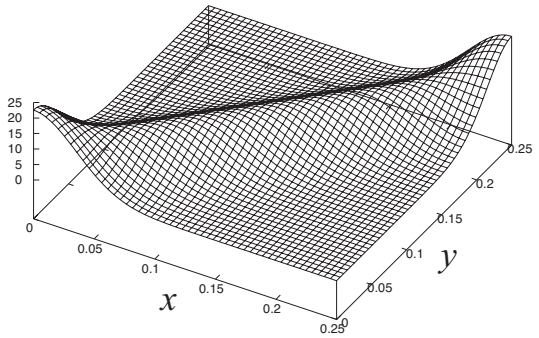

Figure 2: Graph of the kernel $\Phi_{approx}(x,y)$ with $k(x,y) = \frac{1}{\alpha}e^{-\beta(x-y)^2}$. The horizontal axis and the depth mean x and y, respectively. Here, we set $\alpha = 0.088623$, $\beta = 400$ and $L = 0.25$.

In [14], Pueyo et al. proposed the model (1), and they discussed the relation between spatial patterns and biomass, and the effects of plant dispersal strategies, fecundity and establishment ability. It is said that there are several factors to desertification. For example, overgrazing, climate change, overuse of water for agriculture, etc. In this paper, we discuss the relation between spatial vegetation patterns and the rainfall rate, which is deeply related to climate change, and the relation between spatial vegetation patterns and the plant loss, which is linked for example with overgrazing. On the basis of these discussions, we first argue the existence and uniqueness of a solution to the system (2) under the Neumann boundary conditions and suitable initial functions.

The paper is organized as follows. In Section 2, we prove the well-posedness of the nonlocal system (2) by using the Schauder fixed point theorem and a comparison principle argument. In Section 3 we identify, depending on the values of parameters, three regimes: extremely and very arid ecosystems both leading to extinction of plants, in contrast with arid ecosystems possibly leading to patchy patterns. In Section 4, we perform computer-aided analysis to shed light on bifurcations from constant to heterogeneous steady states, that are natural candidates to describe patchiness. Finally, we give some concluding remarks in Section 5.

2 Well-posedness of the nonlocal system

In this section we prove, under suitable assumptions, the well-posedness of the nonlocal system (2) equipped with the no flux boundary conditions for surface water and soil water.

For this analysis, let us use the small letters u, w, p, and then consider

$$\begin{cases} \partial_t u - \Delta u = r - gH(p)u & t>0,\ x\in\Omega,\\ \partial_t w - d\Delta w + e_0 w = H(p)u - K(w)p & t>0,\ x\in\Omega,\\ \partial_t p + bp = aK(w)p + M(w)c\displaystyle\int_\Omega \Phi(x,y)p(t,y)\,dy & t>0,\ x\in\Omega,\\ (u(0,x),w(0,x),p(0,x)) = (u_0(x),w_0(x),p_0(x)) & x\in\Omega,\\ \left(\frac{\partial u}{\partial \nu}(t,x),\frac{\partial w}{\partial \nu}(t,x)\right) = (0,0) & t>0,\ x\in\partial\Omega, \end{cases} \tag{6}$$

where r, g, d, e_0, b, a and c are positive constants. To stick with (2) we could select $H(p) = \frac{p+w_U}{p+1}$, $K(w) = M(w) = \frac{w}{w+1}$, but we allow more profiles by only making the following assumptions.

Assumption 2.1 (Nonlinear functions) *Functions H, K, M are increasing and locally Lipschitz continuous on $[0,\infty)$ and satisfy, for some constants H^+, K^+, M^+,*

$$0 < H(0) \le H(p) \le H^+ \quad \text{for all } p\ge 0, \tag{7}$$

$$0 = K(0) < K(w) \le K^+ \quad \text{for all } w>0, \tag{8}$$

$$0 = M(0) < M(w) \le M^+ \quad \text{for all } w>0. \tag{9}$$

As far as initial conditions are concerned, our assumptions are the following.

Assumption 2.2 (Initial conditions) *The initial data (u_0,v_0,p_0) are smooth, nonnegative, $p_0\not\equiv 0$, and satisfy the expected compatibility conditions that is $\left(\frac{\partial u_0}{\partial \nu}(x),\frac{\partial w_0}{\partial \nu}(x)\right) = (0,0)$, for all $x\in\partial\Omega$.*

We start with some useful *a priori* estimates. In the sequel, for $T>0$, we define $Q_T := (0,T)\times\Omega$.

Lemma 2.3 (A priori estimates) *Let Assumptions 2.1, 2.2 and 1.1 hold. Then, for any $T>0$, there is a constant $C>0$ such that any nonnegative solution $(u,w,p)\in C(\overline{Q_T})^3$ of the nonlocal system (6) satisfies*

$$0\le u(t,x),\ w(t,x),\ p(t,x)\le C \quad \text{for all } (t,x)\in\overline{Q_T}.$$

Proof. • Notice that the constants 0 and $\frac{r}{gH(0)}$ are sub- and super-solutions for equation $\partial_t u - \Delta u = r - gH(p)u$, therefore it follows from the parabolic maximum principle that

$$0 \le u(t,x) \le C_u := \max\left(\frac{r}{gH(0)}, \|u_0\|_{L^\infty(\Omega)}\right), \tag{10}$$

and $u(t,x) > 0$ as soon as $t > 0$, $x \in \Omega$, thanks to the strong maximum principle.

• The above control on u then implies that the constants 0 and H^+C_u/e_0 are sub- and super-solutions for equation $\partial_t w - d\Delta w + e_0 w = H(p)u - K(w)p$, and therefore

$$0 \le w(t,x) \le C_w := \max\left(\frac{H^+C_u}{e_0}, \|w_0\|_{L^\infty(\Omega)}\right), \tag{11}$$

and $w(t,x) > 0$ as soon as $t > 0$, $x \in \Omega$, thanks to the strong maximum principle.

• To prove the nonnegativity of p, we write

$$\partial_t p + (b - aK(w(t,x)))p = \theta(t,x) := M(w(t,x))c\int_\Omega \Phi(x,y)p(t,y)\,dy, \tag{12}$$

which we regard as a first order ODE (with x playing the role of a parameter), so that we have the implicit formula

$$p(t,x) = e^{-bt+a\int_0^t K(w(\tau,x))\,d\tau}\left(p_0(x) + \int_0^t e^{b\tau - a\int_0^\tau K(w(h,x))\,dh}\theta(\tau,x)\,d\tau\right). \tag{13}$$

In particular, for any $x \in \overline{\Omega}$, the continuity of $p(\cdot,x)$, $K(w(\cdot,x))$ and $M(w(\cdot,x))$ on $[0,T]$ enforces the partial application $t \mapsto p(t,x)$ to belong to $C^1([0,T])$. We claim that, for any $x \in \overline{\Omega}$, we can define

$$t_x := \sup\{t \in (0,T] : 0 < \tau < t \Longrightarrow p(\tau,x) > 0\} \in (0,T]. \tag{14}$$

Indeed, if $p(0,x) = p_0(x) > 0$ this is trivial. On the other hand, if $p(0,x) = p_0(x) = 0$, evaluating (12) at point $(0,x)$ yields

$$\partial_t p(0,x) = M(w_0(x))c\int_\Omega \Phi(x,y)p_0(y)\,dy,$$

which is strictly positive — in view of $p_0 \ge 0$, $p_0 \not\equiv 0$ and (3)— which also validates definition (14). The function $x \mapsto t_x$ being lower semi continuous on the compact $\overline{\Omega}$, we can define

$$T^* := \min_{x\in\overline{\Omega}} t_x \in (0,T].$$

Let us assume, by way of contradiction, that $T^* < T$. Then, for a x^* such that $T^* = t_{x^*}$, we have $p(T^*,x^*) = 0$ so that, by evaluating (13) at point (T^*,x^*), we get that $p_0(x^*) = 0$ and $\theta(\tau,x^*) = M(w(\tau,x^*))c\ \int_\Omega \Phi(x^*,y)p(\tau,y)\,dy = 0$ for all $0 \le \tau \le T^*$. In view of (9), $M(w(\tau,x^*)) > 0$ as soon as $\tau > 0$ so that

$$\int_\Omega \Phi(x^*,y)p(\tau,y)\,dy = 0 \quad \text{ for all } 0 < \tau \le T^*.$$

This, combined with assumption (3), enforces $p(\tau,y) = 0$ for all (τ,y) in the cylinder $[0,T^*]\times B(x^*,\delta_\Phi)$. By repeating such a procedure, we can cover the compact region $\overline{Q_{T^*}}$ by a finite

number of such cylinders and discover $p \equiv 0$ on $\overline{Q_{T^*}}$, which contradicts $p_0 \not\equiv 0$. As a result, $T^* = T$ and the nonnegativity of p is proved. We have even proved that $p(t,x) > 0$ as soon as $t > 0$, $x \in \overline{\Omega}$.

• It remains to bound p from above. The equation for p in (6) yields

$$\partial_t p(t,x) \leq (aK^+ - b)p(t,x) + M^+ c \int_\Omega \Phi(x,y)p(t,y)\,dy. \tag{15}$$

Defining the total mass of plants $P(t) := \int_\Omega p(t,x)\,dx$, integrating the above inequality over $x \in \Omega$, using Fubini-Tonelli theorem and (4) we obtain $P'(t) \leq \beta P(t)$, where

$$\beta := aK^+ - b + M^+ c =: \delta + M^+ c. \tag{16}$$

It therefore follows that $P(t) \leq P(0)e^{\beta t}$ which we plug into (15) to get the differential inequality

$$\partial_t p(t,x) \leq \delta p(t,x) + M^+ c \Phi_{max} P(0) e^{\beta t}, \quad p(0,x) = p_0(x). \tag{17}$$

Since $(p_0(x) - \Phi_{max}P(0))\,e^{\delta t} + \Phi_{max}P(0)e^{\beta t}$ is the solution of the equation associated naturally with (17), we get by comparison that

$$\begin{aligned} p(t,x) &\leq (p_0(x) - \Phi_{max}P(0))\,e^{\delta t} + \Phi_{max}P(0)e^{\beta t} \\ &\leq (\|p_0\|_{L^\infty(\Omega)} + \Phi_{max}P(0))e^{\beta t} \\ &\leq (\|p_0\|_{L^\infty(\Omega)} + \Phi_{max}P(0))\max(1, e^{\beta T}) =: C_p, \end{aligned} \tag{18}$$

which concludes the proof of the lemma. □

Remark 2.4 (Extremely arid ecosytems) *If the constant $\beta = aK^+ - b + M^+c$ turns out to be negative, then there is $C > 0$ such that, for all $x \in \Omega$,*

$$p(t,x) \leq Ce^{\beta t} \to 0, \qquad \text{as } t \to \infty,$$

that is an exponentially fast extinction of plants.

We now prove the well-posedness of problem (6) by using the Schauder fixed point theorem.

Theorem 2.5 (Well-posedness of the nonlocal system) *Let Assumptions 2.1, 2.2 and 1.1 hold. Then, for any $T > 0$, the nonlocal problem* (6) *has a unique nonnegative solution (u,w,p) in $C^{\frac{1+\alpha}{2},1+\alpha}(\overline{Q_T}) \times C^{\frac{1+\alpha}{2},1+\alpha}(\overline{Q_T}) \times (C(\overline{Q_T}) \cap C_t^1(\overline{Q_T}))$ for any $0 < \alpha < 1$.*

Proof. Let $T > 0$ be given. Let us define a convex and closed subset of $X := C(\overline{Q_T})^3$ by

$$A := \left\{ (u,w,p) \in X :\ 0 \leq u,w,p \leq C,\ (u,w,p)(0,x) = (u_0,w_0,p_0)(x),\ P(t) \leq P(0)e^{\beta t} \right\},$$

where $C := \max(C_u, C_w, C_p)$ (see (10), (11), (18) in proof of Lemma 2.3), $P(t) := \int_\Omega p(t,x)\,dx$ and β is defined in (16). Let $(u,w,p) \in A$ be given.

• We denote by $\bar{u}$ the solution of the linear (observe that the initially given p is plugged in the right hand side member) parabolic problem

$$\begin{cases} \partial_t \bar{u} - \Delta \bar{u} = r - gH(p)\bar{u} & t > 0,\ x \in \Omega, \\ \bar{u}(0,x) = u_0(x) & x \in \Omega, \\ \frac{\partial \bar{u}}{\partial \nu}(t,x) = 0 & t > 0,\ x \in \partial\Omega. \end{cases} \tag{19}$$

We have $0 \le \bar{u} \le C_u$ (see proof of Lemma 2.3) and it follows from standard parabolic estimates (see e.g. [10]) that

$$\|\bar{u}\|_{C^{\frac{1+\alpha}{2},1+\alpha}(\overline{Q_T})} \le \overline{C_u}, \tag{20}$$

where $\overline{C_u}$ does not depend on $(u,w,p) \in A$ but only on C, T, $|\Omega|$, r, g, H^+.

• We also denote by $\bar{w}$ the solution of the nonlinear parabolic problem (observe that the $\bar{u}$ obtain previously — and not the initially given u— is plugged in the right-hand side member to insure that C_w remains a super-solution)

$$\begin{cases} \partial_t \bar{w} - d\Delta \bar{w} + e_0 \bar{w} = H(p)\bar{u} - K(\bar{w})p & t > 0,\ x \in \Omega, \\ \bar{w}(0,x) = w_0(x) & x \in \Omega, \\ \frac{\partial \bar{w}}{\partial \nu}(t,x) = 0 & t > 0,\ x \in \partial\Omega. \end{cases} \tag{21}$$

Notice that the existence of $\bar{w}$ is guaranteed (see [22, Chapter 14]) by the *a priori* estimate $0 \le \bar{w} \le C_w$ (see proof of Lemma 2.3). It follows from standard parabolic estimates that

$$\|\bar{w}\|_{C^{\frac{1+\alpha}{2},1+\alpha}(\overline{Q_T})} \le \overline{C_w}, \tag{22}$$

where $\overline{C_w}$ does not depend on $(u,w,p) \in A$ but only on C, T, $|\Omega|$, d, e_0, H^+, K^+.

• Last we denote by $\bar{p}$ the solution of the first order ODE, with x playing the role of a parameter, (observe that the initially given p and the previously obtained $\bar{w}$ — and not the initially given w— are plugged in the right hand side member; see below for an explanation of this choice)

$$\begin{cases} \partial_t \bar{p} + (b - aK(\bar{w}(t,x)))\bar{p} = \theta(t,x) := M(\bar{w}(t,x))c \displaystyle\int_\Omega \Phi(x,y)p(t,y)\,dy \\ \bar{p}(0,x) = p_0(x), \end{cases} \tag{23}$$

that is

$$\bar{p}(t,x) = e^{-bt + a\int_0^t K(\bar{w}(\tau,x))\,d\tau} \left(p_0(x) + \int_0^t e^{b\tau - a\int_0^\tau K(\bar{w}(h,x))\,dh} \theta(\tau,x)\,d\tau \right). \tag{24}$$

The nonnegativity of p implies that of $\bar{p}$. Having inserted the control $P(t) \le P(0)e^{\beta t}$ in the definition of the set A allows to recover $\bar{p} \le C_p \le C$. Indeed, the analogous of (15), that is

$$\partial_t \bar{p}(t,x) \le (aK^+ - b)\bar{p}(t,x) + M^+ c \int_\Omega \Phi(x,y)p(t,y)\,dy, \tag{25}$$

combined with $P(t) \le P(0)e^{\beta t}$ implies the analogous of (17) for $\bar{p}$, which implies $\bar{p} \le C_p$ as in the proof of Lemma 2.3. On the other hand, we need to show that the control $\bar{P}(t) := \int_\Omega \bar{p}(t,x)\,dx \le P(0)e^{\beta t}$ has not been lost. Integrating (25) over $x \in \Omega$, using Fubini-Tonelli theorem and (4) we obtain

$$\bar{P}'(t) \le (aK^+ - b)\bar{P}(t) + M^+ cP(t) \le (aK^+ - b)\bar{P}(t) + M^+ cP(0)e^{\beta t}. \tag{26}$$

By the definition of β in (16), $P(0)e^{\beta t}$ solves the equation associated naturally with (26), so that by comparison we get the desired estimate $\bar{P}(t) \le P(0)e^{\beta t}$. We now prove that

$$\{\bar{p} :\ (u,w,p) \in A\} \text{ is relatively compact in } C(\overline{Q_T}), \tag{27}$$

using Arzéla-Ascoli theorem. The uniform boundedness is already known and the equicontinuity follows from the following two facts. First, (23) provides a uniform (w.r.t. $(u,w,p)\in A$, $(t,x)\in\overline{Q_T}$) bound for $|\partial_t\bar{p}(t,x)|$, which settles the case of the time variable. Secondly, the case of the space variable directly follows from the expression (24) and the uniform continuity of M, K, Φ on compact sets, the uniform continuity of p_0 on $\overline{\Omega}$ and the uniform (w.r.t. $(u,w,p)\in A$) bound (22) (notice that this is where we would have faced a problem if we had plugged the initially given w, which is only continuous, rather than $\bar{w}$ into (23)).

• Hence, we are equipped with the continuous operator

$$\mathcal{L}:(u,w,p)\in A\mapsto(\bar{u},\bar{w},\bar{p})\in A,$$

with A a convex and closed subset of the Banach space X. Moreover it follows from estimates (20), (22) and (27) that $\mathcal{L}(A)$ is relatively compact. Therefore, by the Schauder fixed point theorem, the operator $\mathcal{L}$ has a fixed point, that is a solution of the nonlocal problem (6).

• Last, uniqueness follows from an adaptation of classical procedures for local system. If (u_1,w_1,p_1) and (u_2,w_2,p_2) are two solutions then, in virtue of the a priori estimate Lemma 2.3, all components lie in the interval $[0,C]$ on which the nonlinear functions H, K and M are Lipschitz continuous. Substract the equation for u_2 from that for u_1, multiply the result by $u:=u_1-u_2$ and then integrate over the domain Ω. Proceed similarly for other equations, add the three estimates to collect

$$\frac{d}{dt}\int_\Omega(u^2+w^2+p^2)(t,x)dx\le Cst\int_\Omega(u^2+w^2+p^2)(t,x)dx.$$

Then the Gronwall lemma yields $u\equiv w\equiv p\equiv 0$. We skip the details but uniqueness actually also follows from the following stronger property, whose proof is given. □

Proposition 2.6 (Comparison principle) *Let $(u_*,w_*,p_*)\ge(0,0,0)$ and $(u^*,w^*,p^*)\ge(0,0,0)$ be such that*

$$\begin{cases}\partial_t u_*-\Delta u_*-r+gH(p^*)u_*\\ \qquad\le\partial_t u^*-\Delta u^*-r+gH(p_*)u^*\\ \partial_t w_*-d\Delta w_*+e_0w_*-H(p_*)u_*+K(w_*)p^*\\ \qquad\le\partial_t w^*-d\Delta w^*+e_0w^*-H(p^*)u^*+K(w^*)p_*\\ \partial_t p_*+bp_*-aK(w_*)p_*-M(w_*)c\displaystyle\int_\Omega\Phi(x,y)p_*(t,y)\,dy\\ \qquad\le\partial_t p^*+bp^*-aK(w^*)p^*-M(w^*)c\displaystyle\int_\Omega\Phi(x,y)p^*(t,y)\,dy,\end{cases}\tag{28}$$

together with $(u_*,w_*,p_*)(0,\cdot)\le(u^*,w^*,p^*)(0,\cdot)$ in Ω, and $(\frac{\partial u_*}{\partial\nu},\frac{\partial w_*}{\partial\nu})\le(\frac{\partial u^*}{\partial\nu},\frac{\partial w^*}{\partial\nu})$ in $(0,T)\times\partial\Omega$. Then

$$(u_*,w_*,p_*)\le(u^*,w^*,p^*)\qquad\text{in }\overline{Q_T}.$$

Proof. Define functions $u:=u_*-u^*$, $w:=w_*-w^*$, $p:=p_*-p^*$. Denote by $L>0$ an upper bound for the Lipschitz constants of H, K and M on the interval $[0,C]$, in which u_*, w_*, p_*, u^*, w^*, p^* take their values. Multiplying the first inequality of (28) by $u^+:=\max(u,0)$,

integrating over $Q_t = (0,t)\times\Omega$, using $u^+(0,\cdot)\equiv 0$, using $\int_\Omega u^+\Delta u \le -\int_\Omega |\nabla u^+|^2$ thanks to $\frac{\partial u}{\partial \nu}(t,\cdot)\le 0$ on $\partial\Omega$, we get

$$\frac{1}{2}\int_\Omega (u^+)^2(t,x)\,dx \le \int_0^t\int_\Omega g(H(p_*)u^* - H(p^*)u_*)u^+.$$

We distinguish three different cases to estimate the integrand in the right hand side member above: if $u_* \le u^*$ it is zero; if $u_* > u^*$ and $p^* \ge p_*$ it is non positive by the monotonicity of H and the nonnegativity of u_* and u^*; if $u_* > u^*$ and $p^* < p_*$ then it is controlled by $g(LCp^+ + H^+u^+)u^+$, since in this case $|p| = p^+$, and hence by $C_1((p^+)^2 + (u^+)^2)$. As a result we have

$$\int_\Omega (u^+)^2(t,x)\,dx \le C_1\int_0^t\int_\Omega ((u^+)^2 + (p^+)^2)(\tau,x)\,dxd\tau. \tag{29}$$

Similar arguments (multiply by w^+, integrate, distinguish cases, use monotonicity and positivity) for the second inequality of (28) lead to

$$\int_\Omega (w^+)^2(t,x)\,dx \le C_2\int_0^t\int_\Omega ((w^+)^2 + (p^+)^2 + (u^+)^2)(\tau,x)\,dxd\tau, \tag{30}$$

with C_2 a constant depending on L, C, H^+ and K^+. For the third inequality of (28), we combine similar arguments with

$$\begin{aligned}\int_\Omega\int_\Omega \Phi(x,y)p(\tau,y)p^+(\tau,x)\,dxdy &\le \Phi_{max}\int_\Omega\int_\Omega p^+(\tau,y)p^+(\tau,x)\,dxdy\\ &\le \Phi_{max}\left(\int_\Omega p^+(\tau,x)\,dx\right)^2 \le \Phi_{max}|\Omega|\int_\Omega (p^+)^2(\tau,x)\,dx,\end{aligned}$$

to derive

$$\int_\Omega (p^+)^2(t,x)\,dx \le C_3\int_0^t\int_\Omega ((p^+)^2 + (w^+)^2)(\tau,x)\,dxd\tau, \tag{31}$$

with C_3 a constant depending on L, C, K^+, M^+, Φ_{max} and $|\Omega|$. Adding (29), (30) and (31), and using the Gronwall lemma we get that

$$\int_\Omega ((u^+)^2 + (w^+)^2 + (p^+)^2)(t,x)\,dx = 0, \qquad \text{for all } 0\le t\le T.$$

Hence, $u^+ = w^+ = p^+ \equiv 0$ on $\overline{Q_T}$, and the comparison principle is proved. □

3 Identification of various regimes

In this section, we formally identify various behaviors for problem (6) depending on the value of the parameters. Recall that β was defined in (16).

Extremely arid ecosystems: $\beta < 0$. As seen in Remark 2.4, $\beta < 0$ leads to an exponentially fast extinction of plants. In the sequel we exclude this situation and assume $\beta > 0$.

Let us investigate the steady states of problem (6), namely nonnegative solutions of

$$\begin{cases} -\Delta u = r - gH(p)u & x \in \Omega, \\ -d\Delta w + e_0 w = H(p)u - K(w)p & x \in \Omega, \\ bp = aK(w)p + M(w)c \displaystyle\int_\Omega \Phi(x,y)p(t,y)\,dy & x \in \Omega, \\ (\frac{\partial u}{\partial \nu}(x), \frac{\partial w}{\partial \nu}(x)) = (0,0) & x \in \partial\Omega. \end{cases} \tag{32}$$

When looking after solutions (u, w, p) with constant p, the third equation yields $p \equiv 0$ or $b = aK(w) + M(w)c$. The former gives $(u_0 \equiv \frac{r}{gH(0)}, w_0 \equiv \frac{r}{ge_0}, p_0 \equiv 0)$. As far as the latter is concerned, since $\beta > 0$ and since K and M are increasing,

$$\exists!\, w_1 > 0,\ aK(w_1) + M(w_1)c = b, \tag{33}$$

which gives $\left(u_1 \equiv \frac{r}{gH(p_1)}, w_1, p_1 \equiv \frac{\frac{r}{g} - e_0 w_1}{K(w_1)}\right)$, whose nonnegativity is to be discussed.

Very arid ecosystems: $\beta > 0$, $\frac{r}{g} < e_0 w_1$. In this context, (u_0, w_0, p_0) is the only nonnegative steady state with constant p. To study its linear stability, let us consider the associated eigenvalue problem (plug $(u, w, p)(t, x) = (u_0, w_0, p_0 \equiv 0) + \varepsilon e^{-\lambda_0 t}(\varphi, \psi, \theta)(x)$ into the parabolic problem and keep the ε terms)

$$\begin{cases} -\lambda_0\varphi - \Delta\varphi = -gH(0)\varphi - r\frac{H'(0)}{H(0)}\theta & x \in \Omega, \\ -\lambda_0\psi - d\Delta\psi + e_0\psi = H(0)\varphi + \frac{r}{g}\frac{H'(0)}{H(0)}\theta - K(\frac{r}{ge_0})\theta & x \in \Omega, \\ -\lambda_0\theta + b\theta = aK(\frac{r}{ge_0})\theta + M(\frac{r}{ge_0})c\displaystyle\int_\Omega \Phi(x,y)\theta(y)\,dy & x \in \Omega, \\ (\frac{\partial\varphi}{\partial\nu}(x), \frac{\partial\psi}{\partial\nu}(x)) = (0,0) & x \in \partial\Omega. \end{cases} \tag{34}$$

Integrating the third equation over $x \in \Omega$, using Fubini-Tonelli theorem and (4) gives

$$\lambda_0 = b - aK(\frac{r}{ge_0}) - M(\frac{r}{ge_0})c. \tag{35}$$

Since $\frac{r}{ge_0} < w_1$, we have $\lambda_0 > b - aK(w_1) - M(w_1)c = 0$, so that $(u_0, w_0, p_0 \equiv 0)$ is linearly stable. As far as the eigenfunction is concerned, notice that plugging (35) yields

$$\int_\Omega \Phi(x,y)(\theta(y) - \theta(x))\,dy = 0, \quad \forall x \in \Omega.$$

Taking a point x where θ reaches its maximum and using (3), we see that θ is constant on a small neighborhood of given size of x and then, by repeating, on the whole of Ω.

The above suggests that, in these very arid ecosystems, we again have an exponentially fast extinction of plants.

Arid ecosystems: $\beta > 0$, $\frac{r}{g} > e_0 w_1$. In this context, (u_0, w_0, p_0) and (u_1, w_1, p_1) are the two nonnegative steady states with constant p. In this regime we have $\lambda_0 < 0$ so that (u_0, w_0, p_0)

is linearly unstable. We now investigate the linear stability of (u_1, w_1, p_1) by looking at the eigenvalue problem

$$\begin{cases} -\lambda_1\varphi - \Delta\varphi = -gH(p_1)\varphi - r\frac{H'(p_1)}{H(p_1)}\theta & x \in \Omega, \\ -\lambda_1\psi - d\Delta\psi + e_0\psi = H(p_1)\varphi + \frac{r}{g}\frac{H'(p_1)}{H(p_1)}\theta - K(w_1)\theta - p_1K'(w_1)\psi & x \in \Omega, \\ -\lambda_1\theta + b\theta = aK(w_1)\theta + aK'(w_1)p_1\psi & \\ \qquad\qquad + M(w_1)c\displaystyle\int_\Omega \Phi(x,y)\theta(y)\,dy + M'(w_1)cp_1\psi & x \in \Omega, \\ (\frac{\partial\varphi}{\partial\nu}(x), \frac{\partial\psi}{\partial\nu}(x)) = (0,0) & x \in \partial\Omega. \end{cases} \tag{36}$$

Integrating the third equation over $x \in \Omega$, using Fubini-Tonelli theorem and (33) yields

$$-\lambda_1 \int_\Omega \theta = (aK'(w_1) + M'(w_1)c)p_1 \int_\Omega \psi,$$

so that $\lambda_1 < 0$ (since principal eigenfunctions are positive), so that p_1 is linearly unstable.

The above suggests that, in these arid ecosystems, there exists in between $p_0 \equiv 0$ and $p_1 > 0$ a nonconstant steady state $p^*(x)$ (possibly spots, stripes...). This will be numerically investigated in subsection 4.2.

4 Steady states

In Section 2, we proved the existence and uniqueness of a global solution to problem (6). Section 3 gave formal discussion on behaviors for problem (6) in some parameter regimes. Then, our subsequent question arises as follows: what kind of solutions do the system (2) exhibit from pattern formation point of view? Since we are interested in vegetation patterns arising in the system, we treat the stationary problem for (2) in this section.

4.1 Constant steady states

We first consider constant equilibrium solutions in the following ODE system associated with (2) (the mean field model):

$$\begin{aligned} \frac{dP}{dt} &= a\frac{W}{W+1}P - bP + c\frac{W}{W+1}P, \\ \frac{dW}{dt} &= U\frac{P+w_U}{P+1} - \frac{W}{W+1}P - e_0W, \\ \frac{dU}{dt} &= r - gU\frac{P+w_U}{P+1}. \end{aligned} \tag{37}$$

Equilibrium points of (37) are computed as

$$(P_0, W_0, U_0) := (0, \frac{r}{e_0 g}, \frac{r}{w_U g})$$

and

$$(P_1, W_1, U_1) := \left(\left(\frac{r}{g} - e_0W_1\right)\frac{W_1+1}{W_1}, \frac{b}{a+c-b}, \frac{r(P_1+1)}{g(P_1+w_U)}\right).$$

Since negative equilibria are ecologically meaningless, we focus on nonnegative ones. The equilibrium point (P_0, W_0, U_0) which indicates desert (bare) states always exists, on the other hand, the existence of the other equilibrium point (P_1, W_1, U_1) depends on the parameter values, which means that the equilibrium point (P_1, W_1, U_1) can be negative according to the parameter setting. For example, when the value of r is small, the plant density P_1 becomes negative. If $P_1 > 0$, then (P_1, W_1, U_1) indicates vegetation states.

We are interested in the transition of vegetation states when the rainfall rate r varies, because it is one of the important parameters to discuss the possibility of desertification in (2). So, we set r as a bifurcation parameter. Figure 3 shows bifurcation diagrams of equilibrium points for (37) when the rainfall r globally varies. One can see from Figure 3

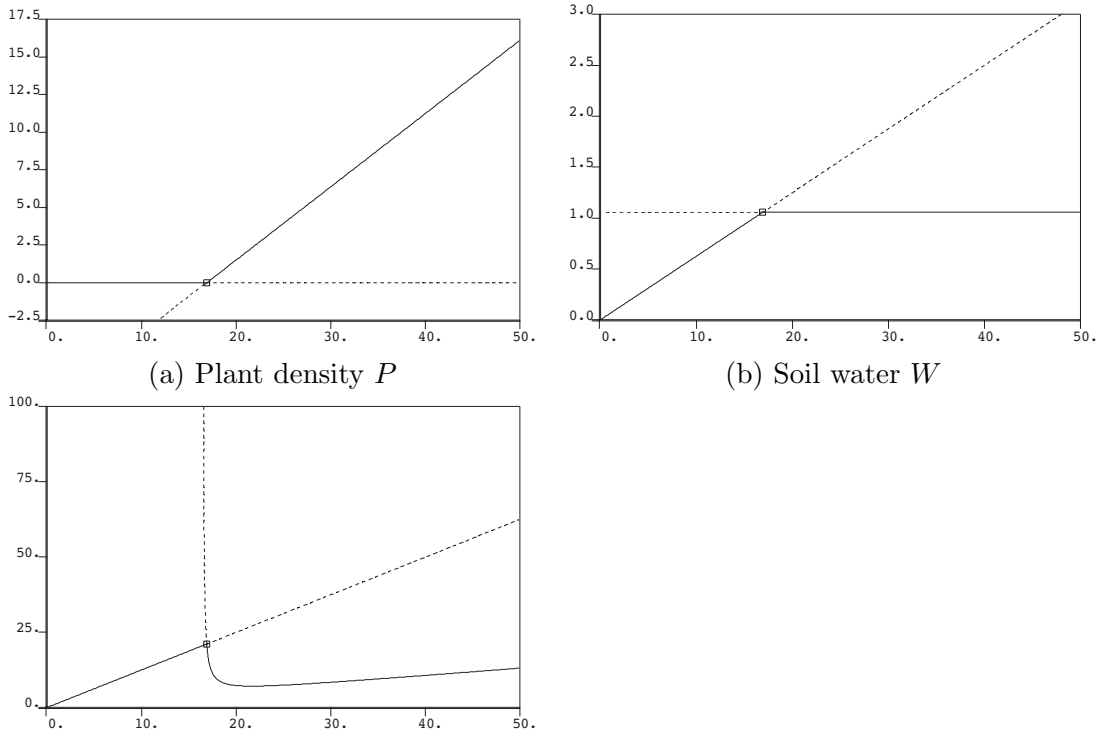

(a) Plant density P

(b) Soil water W

(c) Surface water U

Figure 3: Structure of equilibrium points of (37). (a) Plant density P. (b) Soil water W. (c) Surface water U. The horizontal and vertical axes mean the parameter r and the value of the component. The solid and dashed curves in the figures mean respectively stable and unstable branches. The mark $\square$ in the figure denotes a bifurcation point. The parameter values are $a = 10$, $b = 5.2$, $c = 0.12$, $e_0 = 4$, $g = 4$ and $w_U = 0.2$.

that $(P_0, W_0, U_0) = (0, \frac{r}{e_0 g}, \frac{r}{w_U g})$, which coincides with bare soil states, is stable for small r, but when the value of r increases, it is destabilized at $r = r_c = 16.9106\cdots$ and another branch which corresponds to $(P_1, W_1, U_1) = ((\frac{r}{g} - e_0 W_1)\frac{W_1+1}{W_1}, \frac{b}{a+c-b}, \frac{r(P_1+1)}{g(P_1+w_U)})$ appears as a consequence of a transcritical bifurcation. The positive part of the branch in Figure 3 (a) corresponds to a vegetated state and it grows linearly as the rainfall rate r increases.

Our original interest is the occurrence of spatial vegetation patterns when the spatial terms are included in the model. Therefore, in the next subsection, we investigate the stability of

the positive equilibrium solution for (2) in one space dimension from the view point of the linear stability analysis, and a transition of spatial patterns, depending on a change of the bifurcation parameter r.

4.2 Global structure of stationary solutions

In this subsection, we consider the stationary problem in one space dimension

$$\begin{aligned} 0 &= a\frac{W}{W+1}P - bP + c\frac{W}{W+1}\int_0^L P(y)\Phi_{approx}(x,y)dy, \\ 0 &= d\Delta W + U\frac{P+w_U}{P+1} - \frac{W}{W+1}P - e_0 W, \qquad 0<x<L, \\ 0 &= \Delta U + r - gU\frac{P+w_U}{P+1}, \end{aligned} \tag{38}$$

under the Neumann boundary conditions $W_x(0) = W_x(L) = U_x(0) = U_x(L) = 0$. Here, we use the dispersion kernel $\Phi_{approx}(x,y)$ associated with (5) as shown in Figure 2. We expect that heterogeneous vegetation patterns emerge as a consequence of bifurcation from the equilibrium solution $(P_1, W_1, U_1) = ((\frac{r}{g} - e_0 W_1)\frac{W_1+1}{W_1}, \frac{b}{a+c-b}, \frac{r(P_1+1)}{g(P_1+w_U)})$. In order to check this, we first carry out the linear stability analysis around the equilibrium solution. The system (2) is linearized around the equilibrium solution (P_1, W_1, U_1) as follows:

$$\begin{pmatrix} \tilde{P}_t \\ \tilde{W}_t \\ \tilde{U}_t \end{pmatrix} = \begin{pmatrix} c\frac{W_1}{W_1+1}T + a\frac{W_1}{W_1+1} - b & (a+c)\frac{P_1}{(W_1+1)^2} & 0 \\ U_1\frac{1-w_U}{(P_1+1)^2} - \frac{W_1}{W_1+1} & d\frac{\partial^2}{\partial x^2} - \frac{P_1}{(W_1+1)^2} - e_0 & \frac{P_1+w_U}{P_1+1} \\ -gU_1\frac{1-w_U}{(P_1+1)^2} & 0 & \frac{\partial^2}{\partial x^2} - g\frac{P_1+w_U}{P_1+1} \end{pmatrix} \begin{pmatrix} \tilde{P} \\ \tilde{W} \\ \tilde{U} \end{pmatrix}, \tag{39}$$

where T is an operator defined by $(T\tilde{P})(x) = \int_0^L \tilde{P}(y)\Phi_{approx}(x,y)dy$. For the linear stability analysis, it is necessary to know a series of eigenvalues for the operator T. However, they are not obtained by hand, so we numerically compute the eigenvalues ρ_n $(n = 1, 2, \cdots)$ such that $\int_0^L \cos(\frac{n\pi y}{L})\Phi_{approx}(x,y)dy = \rho_n \cos(\frac{n\pi x}{L})$. When we set $\alpha = 0.088623$, $\beta = 400$ and $L = 0.25$, the eigenvalues of the operator T are obtained as follows:

$$\begin{aligned} &\rho_1 = 0.906017, \quad &&\rho_2 = 0.673822, \quad &&\rho_3 = 0.411369, \quad &&\rho_4 = 0.206149, \\ &\rho_5 = 0.084802, \quad &&\rho_6 = 0.028637, \quad &&\rho_7 = 0.007938, \quad &&\rho_8 = 0.001806, \\ &\rho_9 = 0.000337, \quad &&\rho_{10} = 0.000052, \quad &&\cdots . \end{aligned}$$

Therefore, for each Fourier mode, we have a series of linear systems of ordinary differential equations

$$\begin{pmatrix} \tilde{P}_{nt} \\ \tilde{W}_{nt} \\ \tilde{U}_{nt} \end{pmatrix} = \begin{pmatrix} c\frac{W_1}{W_1+1}\rho_n + a\frac{W_1}{W_1+1} - b & (a+c)\frac{P_1}{(W_1+1)^2} & 0 \\ U_1\frac{1-w_U}{(P_1+1)^2} - \frac{W_1}{W_1+1} & -d(\frac{n\pi}{L})^2 - \frac{P_1}{(W_1+1)^2} - e_0 & \frac{P_1+w_U}{P_1+1} \\ -gU_1\frac{1-w_U}{(P_1+1)^2} & 0 & -(\frac{n\pi}{L})^2 - g\frac{P_1+w_U}{P_1+1} \end{pmatrix} \begin{pmatrix} \tilde{P}_n \\ \tilde{W}_n \\ \tilde{U}_n \end{pmatrix},$$

$n = 1, 2, 3, \cdots$. Investigating zero eigenvalues of these linearized matrices, we know the location of bifurcation points on the constant solution branch (P_1, W_1, U_1). When we focus on the parameters r and d, a bifurcation curve for n mode, where an eigenvalue takes zero,

is obtained as

$$\begin{aligned}\Gamma_n =&\{(r,d)\in\mathbb{R}^2 \mid \\ &(c\frac{W_1}{W_1+1}\rho_n + a\frac{W_1}{W_1+1} - b)(d(\frac{n\pi}{L})^2 + \frac{P_1}{(W_1+1)^2} + e_0)((\frac{n\pi}{L})^2 + g\frac{P_1+w_U}{P_1+1}) \\ &+ ((a+c)\frac{P_1}{(W_1+1)^2})(\frac{P_1+w_U}{P_1+1})(-gU_1\frac{1-w_U}{(P_1+1)^2}) \\ &+ ((a+c)\frac{P_1}{(W_1+1)^2})(U_1\frac{1-w_U}{(P_1+1)^2} - \frac{W_1}{W_1+1})((\frac{n\pi}{L})^2 + g\frac{P_1+w_U}{P_1+1}) = 0\}.\end{aligned}$$

Based on the bifurcation curves, we know the stable and unstable regions of the equilibrium solution (P_1, W_1, U_1) in the (r,d)-plane. Figure 4 indicates the bifurcation curves $\{\Gamma_n\}$ and

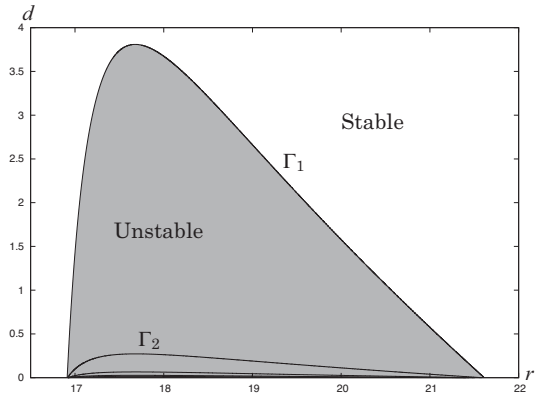

Figure 4: Bifurcation curves, and stable and unstable regions of the constant solution (P_1, W_1, U_1) for (2). The horizontal and vertical axes mean the parameters r and d, respectively. The other parameter values are the same as the ones in Figure 3.

the stable and unstable regions for the equilibrium solution. We can see from the figure that for a suitably fixed value of d, the stability of the equilibrium solution (P_1, W_1, U_1) changes from stable state into unstable one as the value r increases from $r = r_c$. When the value r increases further, it recovers the stability. Moreover, we can expect that the one-mode solution primarily bifurcates from the constant solution branch in this parameter setting when the value of r increases.

Based on Figure 4, we numerically compute a global bifurcation diagram by using a numerical bifurcation software AUTO [3]. Figure 5 shows a bifurcation diagram for $d = 0.1$ when the bifurcation parameter r is globally varied. For small values of r, the bare state $(P_0, W_0, U_0) = (0, \frac{r}{e_0 g}, \frac{r}{w_U g})$ is stable. As the value r increases, the homogeneous vegetation state $(P_1, W_1, U_1) = ((\frac{r}{g} - e_0 W_1)\frac{W_1+1}{W_1}, \frac{b}{a+c-b}, \frac{r(P_1+1)}{g(P_1+w_U)})$ appears stably due to the transcritical bifurcation at $r = r_c = 16.9106\cdots$ while the bare state $(0, \frac{r}{e_0 g}, \frac{r}{w_U g})$ becomes unstable. However, this uniform vegetated branch undergoes a subcritical pitchfork bifurcation at $r = 16.9167\cdots$ and becomes unstable. Although the non-constant branches resulting from the bifurcation point are unstable, they become stable via a saddle-node bifurcation at $r = 15.5772\cdots$ and keeps the stability up to $r = 25.5270\cdots$. And the saddle-node bifurcation at $r = 25.5270\cdots$ changes the stability of the branches and they connect to the constant solution

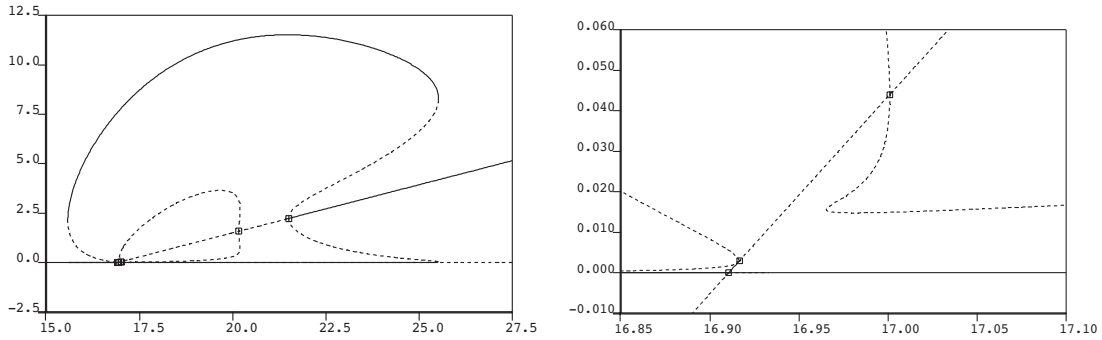

Global bifurcation diagram Enlarged figure

Figure 5: Structure of steady states of (38). The horizontal and vertical axes mean the parameter r and the value of P at $x = 0$. The solid and dashed curves in the figures mean respectively stable and unstable branches. The mark $\square$ in the figure denote a bifurcation point. The parameter values are $a = 10$, $b = 5.2$, $c = 0.12$, $d = 0.1$, $e_0 = 4$, $g = 4$, $w_U = 0.2$ and $L = 0.25$.

branch at $r = 21.5037\cdots$. Here, we note that there appears a pair of nonconstant stationary solution branches as a result of a pitchfork bifurcation, that is the upper and lower branches in Figure 5. Actually, we can identify these two branches because a stationary solution on the lower branch corresponds to $(P(L-x), W(L-x), U(L-x))$ if $(P(x), W(x), U(x))$ is a stationary solution on the upper branch. Therefore, the stability of these two branches coincides. Stable nontrivial stationary solutions observed in the range $15.5772 < r < 25.5270$ correspond to non-constant stable vegetation patterns. In addition, one can see from the figure that there exist bistable regions in $15.5772 < r < 16.9167$ and $21.5037 < r < 25.5270$. That is, there are two stable stationary solutions, a uniform state and a heterogeneous state in these parameter regions. The profiles of stationary solutions for some values of r are shown in Figure 6. We can observe that the amounts of average biomass $\frac{1}{L}\int_0^L P(x)dx$ increase as the rainfall parameter r rises. When the vertical axis $P(0)$ in Figure 5 is replaced by the average biomass $\frac{1}{L}\int_0^L P(x)dx$, the global bifurcation diagram is shown in Figure 7. This figure indicates that the biomass of heteronegenous steady states is always higher than that of constant steady states for each value of r. Therefore, aggregation formation is more reasonable for plants in arid ecosystems than uniform vegetation from the viewpoint of a survival strategy.

Next, we change the bifurcation parameter from r to b in order to investigate a relation between vegetation patterns and plant loss due to overgrazing. Figure 8 shows a global bifurcation diagram when the value of b varies as a bifurcation parameter. In this case, for large values of b, the bare state is stable, while the homogeneous vegetated state is stable for small values of b. We can see that the heterogeneous vegetated patterns appear for the moderate values of b. Therefore, we know from this result that vegetation patterns appear in a self-organized way when the plant loss rate increases. And when the plant loss progresses further due to overgrazing for instance, the land desertifies.

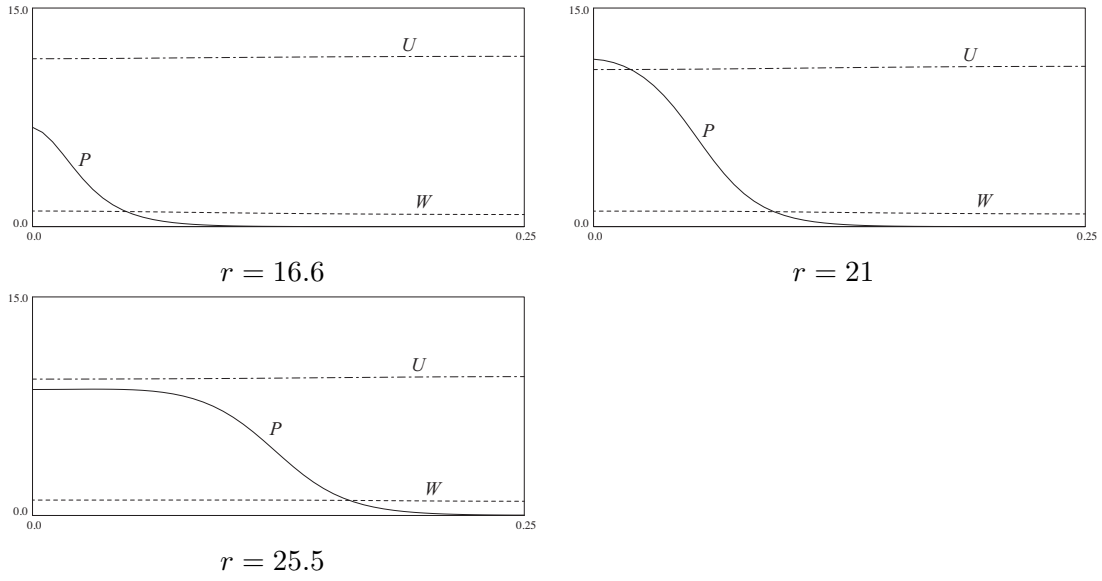

Figure 6: Profiles of non-constant stationary solutions in (38) for some parameter values r. The solid, dashed and long dashed short dashed curves indicate P, W and U, respectively. The other parameter values are the same as the ones in Figure 5.

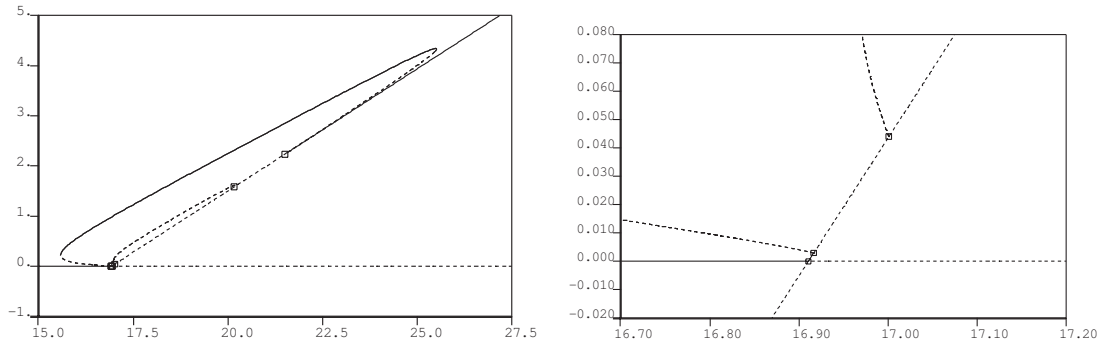

Figure 7: Structure of steady states of (38). The horizontal and vertical axes mean the parameter r and the average mass $\frac{1}{L}\int_0^L P(x)dx$. The parameter values are the same as the ones in Figure 5.

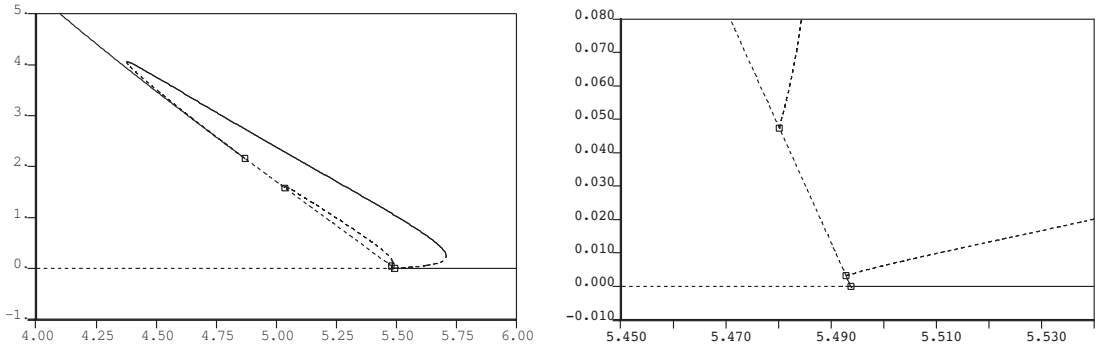

Global bifurcation diagram Enlarged figure

Figure 8: Structure of steady states of (38). The horizontal and vertical axes mean the parameter b and the average mass $\frac{1}{L}\int_0^L P(x)dx$. The parameter values are $a = 10$, $r = 19$, $c = 0.12$, $d = 0.1$, $e_0 = 4$, $g = 4$, $w_U = 0.2$ and $L = 0.25$.

4.3 Global structure of stationary solutions for other kernels

So far, we have discussed global structures of stationary solutions of (38) together with the kernel (5) in one space dimension. However, we have several choices for the kernel $k(x, y)$. In this subsection, we numerically show global structures of stationary solutions for other types of kernels and discuss the variation of bifurcation diagrams according to the choice of kernels. Since the kernel prescribes seed dispersal, we assume that it has a unimodal shape. We here consider the following two types of kernels:

$$k(x, y) = \frac{1}{\alpha} e^{-\beta|x-y|} \tag{40}$$

and

$$k(x, y) = \frac{1}{\alpha} \max\{1 - \beta|x - y|^2, 0\}. \tag{41}$$

The exponential kernel (40) has a cusp and a tail, whereas the quadratic kernel (41) has no tail. We give the global bifurcation diagrams for (38) with (40) and (41) in Figures 9 and 10, respectively. Surprisingly, qualitatively similar bifurcation diagrams to Figures 5 and 7 are obtained. These results suggest that the choice of suitable kernels is not of great influence on the global structure of stationary solutions. That is, if the kernel is a unimodal type, a similar tendency of vegetation patterns may be exhibited.

4.4 Two dimensional vegetation patterns

Next, we consider a transition of vegetation patterns in a two dimensional domain. It is said that there are some factors to desertification (overgrazing, climate change, overuse of water for agriculture, etc). Here, we focus on two parameters and investigate a transition of vegetation patterns when we vary the two parameters. The first is the rainfall rate r, whose parameter is related to climate change. The second case is on the parameter b which means death or removal rate of plant density. This parameter corresponds to grazing livestock. Figure 11 shows vegetation patterns P at $t = 1000$ when the rainfall rate r changes. Here, we compute (2) together with the two dimensional version of (5) under the Neumann boundary

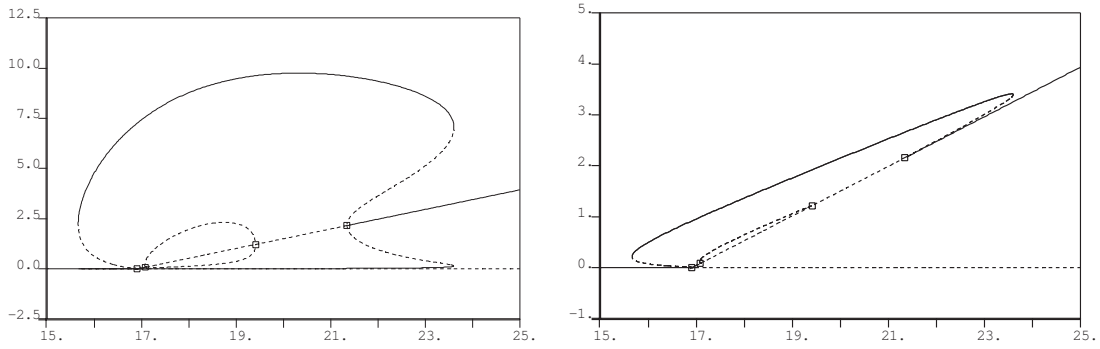

(a) (b)

Figure 9: Structure of constant steady states of (38) with (40). (a) The horizontal and vertical axes are the parameter r and the values of P at $x = 0$, respectivey. (b) The horizontal and vertical axes are the parameter r and the average mass $\frac{1}{L}\int_0^L P(x)dx$, respectivey. The parameter values are $a = 10$, $b = 5.2$, $c = 0.12$, $d = 0.1$, $e_0 = 4$, $g = 4$, $w_U = 0.2$, $\beta = 25$ and $L = 0.25$.

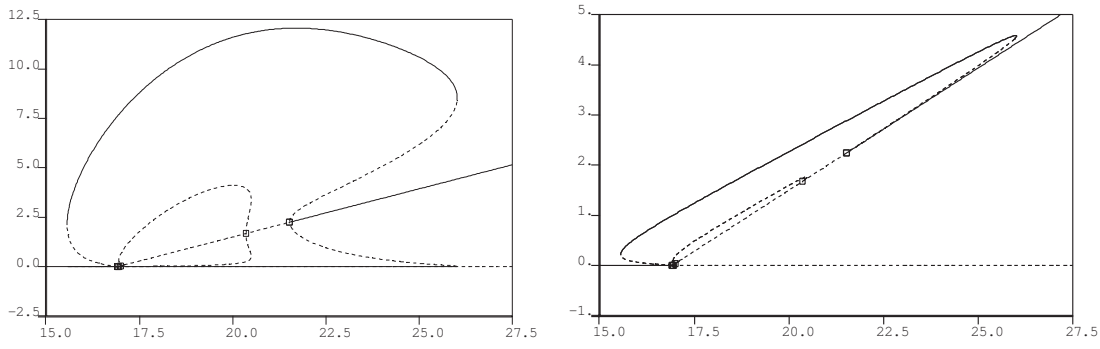

(a) (b)

Figure 10: Structure of constant steady states of (38) with (41). (a) The horizontal and vertical axes are the parameter r and the values of P at $x = 0$, respectivey. (b) The horizontal and vertical axes are the parameter r and the average mass $\frac{1}{L}\int_0^L P(x)dx$, respectivey. The parameter values are $a = 10$, $b = 5.2$, $c = 0.12$, $d = 0.1$, $e_0 = 4$, $g = 4$, $w_U = 0.2$, $\beta = 200$ and $L = 0.25$.

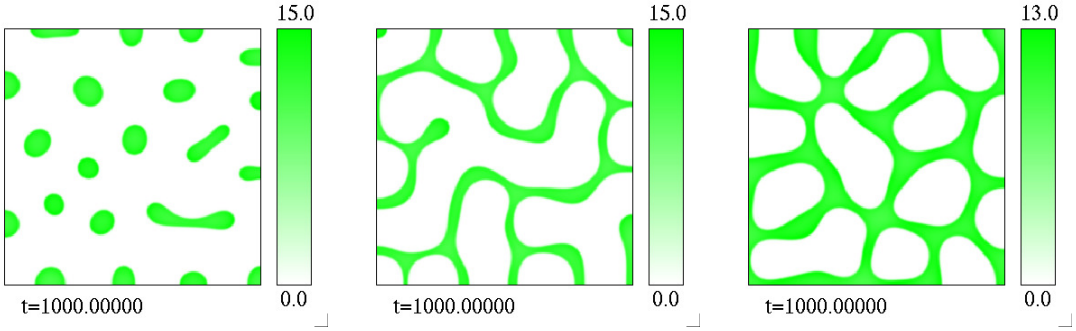

$r = 16.5$ $r = 19$ $r = 22$

Figure 11: Vegetation patterns P on a square domain $(0, 8) \times (0, 8)$ when the value of r varies. The other parameter values are the same as the ones in Figure 5. The color scale indicates that green color corresponds to high plant density and white color corresponds to less plant density.

conditions and initial conditions (P_1, W_1, U_1) with spatially nonuniform perturbations. For large r, we numerically observed uniform vegetation states. As the rate r decreases, the uniform vegetation states are destabilized and gap patterns are observed ($r = 22$). As the value of r decreases further, labyrinth patterns are generated ($r = 19$). For suitably small values of r, spot patterns are formed ($r = 16.5$) and for very small values of r, we no longer observe vegetation states. These results indicate that vegetation patterns change according to the rainfall rate r, which is a good agreement with field observations. When we vary the parameter b, the results are indicated by Figure 12. When the grazing parameter b is suitably

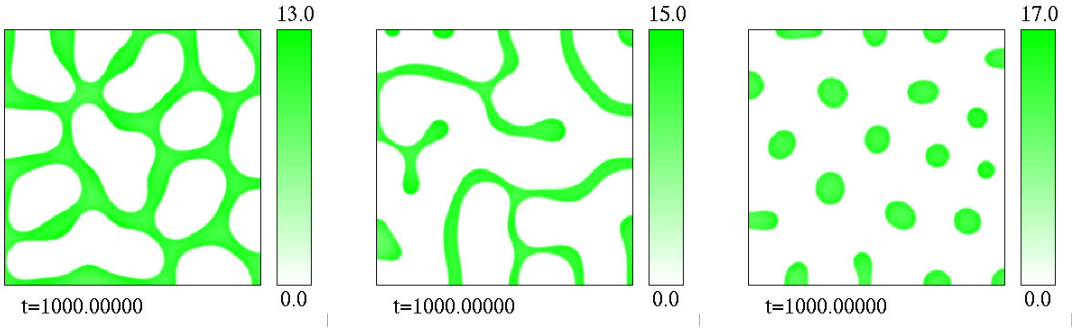

$b = 4.8$ $b = 5.3$ $b = 5.6$

Figure 12: Vegetation patterns P on a square domain $(0, 8) \times (0, 8)$ when the value of b varies. The other parameter values are the same as the ones in Figure 8.

small, we numerically obtained uniform vegetation states. As the parameter b increases, gap, labyrinth and spot patterns are observed as shown in Figure 12.

These results suggest that if the rainfall becomes less due to climate change, or if plant density tend to be exploited due to overgrazing, vegetation in arid ecosystems forms patterns in a self-organized way and as the environmental condition becomes worse, vegetation gener-

ates spot patterns at a crucial state, which implies the occurrence of a catastrophic shift to bare soil.

5 Concluding remarks

In this paper, we have discussed a nonlocal system for vegetation in arid ecosystems: as argued in [14], in order to describe the plant dispersal, it is more reasonable to use a nonlocal term than to use a diffusion term. We have obtained the existence and uniqueness of a global solution, the structure of stationary solutions and two-dimensional patterns. Also, we have several choices for the kernel included in the nonlocal term, but we confirmed that the results for different kernels are qualitatively similar if the kernel shape is of unimodal type. Although the nonlocal system discussed here is not a reaction-diffusion system, non-constant vegetation patterns reminiscent of Turing patterns have been exhibited in a self-organized way. In this regard, understanding of the relation between a nonlocal system and a reaction-diffusion system is progressing [12].

Once land has desertified, it it too difficult to recover it to uniform vegetated states. In Figures 5, 7 and 8, we found that there are bistable regions between the pitchfork bifurcation points on (P_1, W_1, U_1) and the saddle-node bifurcation points on the nonconstant stationary solution branch, namely coexistence of stable homogeneous steady states and stable heterogeneous ones. Therefore, to recover land from desertification state to heterogeneous vegetated states, the rainfall rate more than the pitchfork bifurcation point in Figures 5 and 7 or the grazing rate less than the pitchfork bifurcation point in Figure 8 is required due to the hysterisis structure. Moreover, we find out that further effort is needed to achieve fully vegetated states because of the hysterisis structure of the other side between heterogeneous vegetation states and homogeneous vegetation states. Such a hysterisis structure is observed in the other models. See [4], [17]. Consequently, when vegetation patterns appear, prompt measures should be taken suitably before desertifying.

We point out some controversial points of the nonlocal model. As shown in Figure 3, the plant density P linearly increases as the rainfall rate r increases, which indicates that there is no saturation effect of the plant density in the system. Moreover, the nonlocal model should include different time scales. For example, the time scale of water movement and infiltration should be different from that of plant growth, establishment etc. From these points of view, we think the model could be improved, and further analyses are required.

Acknowledgements

This work was supported by JSPS KAKENHI (HI: Grant Number 17K14237, MM: Grant Number 15K13462).

References

[1] E. J. Allen, L. J. S. Allen and X. Gilliam, *Dispersal and competition models for plants*, J. Math. Biol. **34** (1996) 455–481.

[2] F. Borgogno, P. D'Odorico, F. Laio and L. Ridolfi, *Mathematical models of vegetation pattern formation in ecohydrology*, Reviews of Geophysics **47** (2009) 2007RG000256.

[3] E. J. Doedel, R. C. Paffenroth, A. R. Champneys, T. F. Fairgrieve, Y. A. Kuznetsov, B. E. Oldeman, B. Sandstede and X. Wang, *AUTO2000: Continuation and bifurcation software for ordinary differential equations (with HomCont).*

[4] J. von Hardenberg, E. Meron, M. Shachak and Y. Zarmi, *Diversity of vegetation patterns and desertification*, Phys. Rev. Lett. **87** (2001) 198101.

[5] R. HilleRisLambers, M. Rietkerk, F. van den Bosch, H. H. T. Prins and H. de Kroon, *Vegetation pattern formation in semi-arid grazing systems*, Ecology **82** (2001) 50–61.

[6] V. Hutson, S. Martinez, K. Mischaikow and G. T. Vickers, *The evolution of dispersal*, J. Math. Biol. **47** (2003) 483–517.

[7] B. J. Kealy and D. J. Wollkind, *A nonlinear stability analysis of vegetative Turing pattern formation for an interaction-diffusion plant-surface water model system in an arid flat environment*, Bull. Math. Biol. **74** (2012) 803–833.

[8] S. Kéfi, M. Rietkerk, C. L. Alados, Y. Pueyo, V. P. Papanastasis, A. ElAich and P. C. de Ruiter, *Spatial vegetation patterns and imminent desertification in Mediterranean arid ecosystems*, Nature **449** (2007) 213–217.

[9] C. A. Klausmeier, *Regular and irregular patterns in semiarid vegetation*, Science **284** (1999) 1826–1828.

[10] O. A. Ladyženskaja, V. A. Solonnikov and N. N. Ural'ceva, *Linear and Quasilinear Equations of Parabolic Type*, translated from the Russian by S. Smith. Translations of Mathematical Monographs, Vol. 23. American Mathematical Society, Providence, R.I., 1967.

[11] E. Meron, E. Gilad, J. von Hardenberg, M. Shachak and Y. Zarmi, *Vegetation patterns along a rainfall gradient*, Chaos Solitons Fract. **19** (2004) 367–376.

[12] H. Ninomiya, Y. Tanaka and H. Yamamoto, *Reaction, diffusion and non-local interaction*, J. Math. Biol. (2017) 1–13.

[13] T. Okayasu and Y. Aizawa, *Systematic analysis of periodic vegetation patterns*, Progress of Theoretical Physics **106** (2001) 705–720.

[14] Y. Pueyo, S. Kéfi, C. L. Alados and M. Rietkerk, *Dispersal strategies and spatial organization of vegetation in arid ecosystems*, Oikos **117** (2008) 1522–1532.

[15] M. Rietkerk, P. Ketner, J. Burger, B. Hoorens and H. Olff, *Multiscale soil and vegetation patchiness along a gradient of herbivore impact in a semi-arid grazing system in West Africa*, Plant Ecology **148** (2000) 207–224.

[16] M. Rietkerk and J. van de Koppel, *Regular pattern formation in real ecosystems*, Trends in Ecology & Evolution **23** (2008) 169–175.

[17] M. Rietkerk, S. C. Dekker, P. C. de Ruiter and J. van de Koppel, *Self-organized patchiness and catastrophic shifts in ecosystems*, Science **305** (2004) 1926–1929.

[18] M. Rietkerk, M. C. Boerlijst, F. van Langevelde, R. HilleRisLambers, J. van de Koppel, L. Kumar, H. H. T. Prins and A. M. de Roos, *Self-organization of vegetation in arid ecosystems*, The American Naturalist **160** (2002) 524–530.

[19] M. Scheffer, J. Bascompte, W. A. Brock, V. Brovkin, S. R. Carpenter, V. Dakos, H. Held, E. H. van Nes, M. Rietkerk and G. Sugihara, *Early-warning signals for critical transitions*, Nature **461** (2009) 53–59.

[20] J. A. Sherratt, *When does colonisation of a semi-arid hillslope generate vegetation patterns?*, J. Math. Biol. **73** (2016) 199–226.

[21] K. Siteur, E. Siero, M. B. Eppinga, J. D. M. Rademacher, A. Doelman and M. Rietkerk, *Beyond Turing: The response of patterned ecosystems to environmental change*, Ecological Complexity **20** (2014) 81–96.

[22] J. Smoller, *Shock Waves and Reaction-Diffusion Equations*, Springer-Verlag, New York, 1994.